J. Fluid Mech. (1976), *vol.* 77, *part* 1, *pp.* 185–208
Printed in Great Britain

Coupling of surface and internal gravity waves: a mode coupling model

By KENNETH M. WATSON,
Department of Physics, University of California, Berkeley
BRUCE J. WEST AND BRUCE I. COHEN
Physical Dynamics Inc., P.O. Box 556, La Jolla, California 92038

(Received 28 April 1975 and in revised form 11 March 1976)

A surface-wave/internal-wave mode coupled model is constructed to describe the energy transfer from a linear surface wave field on the ocean to a linear internal wave field. Expressed in terms of action–angle variables the dynamic equations have a particularly useful form and are solved both numerically and in some analytic approximations. The growth time for internal waves generated by the resonant interaction of surface waves is calculated for an equilibrium spectrum of surface waves and for both the Garrett–Munk and two-layer models of the undersea environment. We find energy transfer rates as a function of undersea parameters which are much faster than those based on the constant Brunt–Väisälä model used by Kenyon (1968) and which are consistent with the experiments of Joyce (1974). The modulation of the surface-wave spectrum by internal waves is also calculated, yielding a 'mottled' appearance of the ocean surface similar to that observed in photographs taken from an ERTS1 satellite (Apel *et al.* 1975*b*).

1. Introduction

In this paper we present a surface-wave/internal-wave mode coupled model to describe the generation of internal waves by surface waves. The possible importance of surface waves for the generation of internal waves is mentioned by Phillips (1966, §5.3) and models for this have been studied by Ball (1964), Thorpe (1966), Hasselmann (1966) and Kenyon (1968). Tank experiments to study the interaction of surface and internal waves have been reported by Lewis, Lake & Ko (1974) and by Joyce (1974).

Syntheses of observations of internal waves in the deep ocean have been made by Garrett & Munk (1972*a*, 1975), who have proposed an explicit equilibrium spectrum for internal waves. Suggested sources of energy to drive internal waves are tidal currents, atmospheric pressure and stress fluctuations, and surface waves (see, for example, Thorpe 1975). The relative importance of these mechanisms at various internal wavenumbers is not known at present. If the internal-wave spectrum is not in equilibrium one might anticipate that energy is fed into the spectrum at longer and intermediate wavelengths and cascades by

nonlinear interactions to the shortest internal-wave wavelengths, where it is dissipated by wave breaking.

We simplify the surface-wave/internal-wave dynamics by treating both the surface and internal wave motions in a linear approximation. The nonlinear coupling is treated to the lowest non-vanishing order in §2. To simplify the analysis further we assume (not unrealistically) that the wavenumbers and frequencies of the surface waves studied are large compared with the wavenumbers and frequencies of the internal waves of interest. The resulting dynamics are expressed using action–angle variables, which allow a simple and efficient numerical integration of the equations of motion.

For the purposes of this paper we model the ocean as follows. In the absence of wave motion the surface is assumed to coincide locally with the plane $z = 0$ of a rectangular co-ordinate system. The bottom is assumed to coincide with the plane $z = -B$. In order to use discrete Fourier expansions, a large rectangular ocean area A_0, with periodic boundary conditions, is considered.

The density $\bar{\rho}(z)$ is assumed to have the following characteristics:

$$\bar{\rho}(z) = \rho_0, \text{ a constant, for } -D < z < 0.$$

A thin pycnocline with density change $\delta\rho$ occurs at $z = -D$. For $-B < z < -D$, $\bar{\rho}(z)$ is a monotonically decreasing function of z. We assume that surface wave motion is negligible below $z = -D$.

The Brunt–Väisälä frequency $N(z)$ appears in the equation for the internal waves (see, for example, Phillips 1966, chap. 5) and in the chosen model for the ocean has the values

$$N(z) = \begin{cases} 0, & -D < z < 0, \\ \left[-(g/\rho_0)\dfrac{d\bar{\rho}(z)}{dz}\right]^{\frac{1}{2}}, & -B < z < -D, \end{cases}$$

and

$$\int_{-D-\delta}^{-D+\delta} N^2(z)\,dz = g\,\delta\rho/\rho_0. \tag{1.1}$$

In (1.1), 2δ is a small interval somewhat greater than the thickness of the pycnocline and the quantity g represents the acceleration of gravity.

Although our dynamical equations are obtained for this rather general model, the numerical calculations are based on either of two more specific models. The first is that of Garrett & Munk (1972*a*):

$$N(z) = \begin{cases} 0, & -D < z < 0, \\ N_0 \exp\left[(z+D)/B\right], & -B < z < -D, \end{cases}$$
$$N_0 = 5{\cdot}2 \times 10^{-3}\ \mathrm{s}^{-1}, \quad B = 5\ \mathrm{km}, \quad b = 1{\cdot}2\ \mathrm{km}. \tag{1.2}$$

The internal-wave eigenmodes for this model are obtained and used in the WKB approximation.

The second model which we use is the two-layer model, which is somewhat unrealistic for oceanographic applications but is useful for comparing calculations with a number of water tank experiments. In this model $N(z) = 0$, except near $z = -D$, where

$$\int_{-D-\delta}^{-D+\delta} N^2(z)\,dz = g\,\delta\rho/\rho_0. \tag{1.3}$$

The derivation of the surface-wave/internal-wave coupled mode equations is described in §2 and the equations numerically integrated for the example of the generation of a single internal wave by the interaction of surface waves. A 'cascade' process of energy exchange familiar from laser–plasma coupling is seen to occur for the surface-wave/internal-wave coupling. The rate at which an internal-wave spectrum is generated by a given spectrum of surface waves is calculated in an analytic approximation in §3.

In §4 the calculation an discussion are continued from §3 for an equilibrium surface-wave spectrum using both a dimensional scaling argument and a direct numerical integration of the coupled nonlinear equations. The dependence of the rate of generating internal waves on the mixed-layer thickness D, pycnocline strength $\delta\rho/\rho_0$ and the internal-wave horizontal wavenumber $\mathbf{K}$ for the lowest three internal-wave modes is also studied. We conclude in this section that the energy transfer rates calculated using either the Garrett–Munk or two-layer models of the undersea environment are much greater than those based on the constant Brunt–Väisälä model used by Kenyon (1968). The total energy transfer rate from the surface to the internal-wave spectrum is also calculated and found to be comparable to estimates of the required rate made by Garrett & Munk (1972*b*) and also made by Bell (1975) for generation due to current flow over an irregular bottom.

In §5 the main results and conclusions of the paper are summarized. In addition, application of the surface-wave/internal-wave coupled mode equations to the tank experiments of Lewis *et al.* (1974) and Joyce (1974) are briefly discussed. Also discussed are the results of some numerical calculations of the development of a 'mottled' appearance of the ocean surface in the presence of internal waves [see Apel *et al.* (1975*b*) for satellite photographs of this phenomenon].

2. The coupling of surface and internal waves

The equations describing mutual coupling of surface and internal waves are presented in this section. In the mixed layer, corresponding to $-D < z < 0$, the flow is treated as irrotational and the fluid velocity $\mathbf{u}$ can be expressed as the gradient of a potential $\Phi(\mathbf{r}, z)$. (Here and elsewhere in this paper we let $\mathbf{r} = (x, y)$ represent a vector in the horizontal plane $z = 0$.)

We assume that the internal-wave modes of interest to us have much lower characteristic frequencies and much longer wavelengths than have the surface waves. This suggests writing the velocity potential Φ in the form

$$\Phi(\mathbf{r}, z, t) = \phi_g(\mathbf{r}, z, t) + \phi_i(\mathbf{r}, z, t). \tag{2.1}$$

Here ϕ_g contains the high frequency, high wavenumber components (surface gravity waves) of Φ, and ϕ_i contains the low frequency, low wavenumber components (internal waves) of Φ. Similarly, we can write the vertical displacement ζ of the ocean surface, due to wave motion, as a sum of a high frequency part ζ_g and a low frequency part ζ_i:

$$\zeta(\mathbf{r}, t) = \zeta_g(\mathbf{r}, t) + \zeta_i(\mathbf{r}, t). \tag{2.2}$$

Bernoulli's equation and the kinematic boundary condition on the surface $z = \zeta(\mathbf{r}, t)$ are, respectively,

$$\left.\begin{aligned} \partial\Phi/\partial t + \tfrac{1}{2}(\nabla\Phi)^2 + g\zeta &= 0, \\ \partial\zeta/\partial t + (\nabla_s\Phi)\cdot(\nabla_s\zeta) &= \partial\Phi/\partial z, \end{aligned}\right\} \quad z = \zeta, \tag{2.3}$$

where ∇_s is the two-dimensional gradient operator, i.e. $\nabla_s \equiv (\partial/\partial x, \partial/\partial y)$.

For small amplitude waves the fluid motion below the ocean surface is described by the equation [see, for example, Phillips 1966, chap. 5, equation (5.2.4)]

$$\frac{\partial^2}{\partial t^2}\left(\frac{\partial^2}{\partial z^2} + \nabla_s^2\right) w(\mathbf{r}, z, t) + N^2(z)\,\nabla_s^2 w(\mathbf{r}, z, t) = Q(\mathbf{u}, N). \tag{2.4}$$

Here w is the vertical component of the fluid velocity and N is the Brunt–Väisälä frequency given by (1.1). The effects of the earth's rotation have been neglected in (2.4) because the internal waves that exhibit strong coupling to surface waves in our calculation have frequencies substantially higher than the inertial frequency. (This will be evident from table 1, described in § 3.)

The quantity $Q(\mathbf{u}, N)$ in (2.4) represents the effect of the internal-wave nonlinear terms and is set equal to zero ($Q = 0$) in our analysis. To see that this is justified, we first note that in the mixed layer, corresponding to $-D < z < 0$, $N = 0$ and $\mathbf{u} = \nabla\Phi$. Direct substitution of these values of N and $\mathbf{u}$ into the expression for Q [the explicit form is given by Phillips 1966, equation (5.2.5)] gives

$$Q(\nabla\Phi, 0) = 0, \tag{2.5}$$

which is consistent with our assumption of potential flow in the mixed layer. For $z < -D$ we have assumed the flow associated with surface waves to be negligible. Here too we can set $Q = 0$, to consistently keep only those nonlinear terms which couple surface and internal waves.

Since we have no coupling of surface and internal waves in either the mixed layer or below, it is the surface boundary conditions (2.3) that contain the nonlinear terms responsible for interaction between the two wave systems.

Near the surface, the low frequency fluid velocity associated with internal waves is

$$\mathbf{u}_i(\mathbf{r}, t) = \nabla\phi_i|_{z=0} \equiv \mathbf{U}(\mathbf{r}, t) + \mathbf{e}w_s(\mathbf{r}, t), \tag{2.6}$$

where $\mathbf{U}$ and w_s are the horizontal and vertical surface-current components, respectively, and $\mathbf{e}$ is a unit vector parallel to the z axis. The corresponding high frequency velocity field associated with surface waves is

$$\mathbf{v} = \nabla\phi_g. \tag{2.7}$$

The properties of internal waves permit us to assume that

$$|\mathbf{U}| \gg |w_s|, \quad |\zeta_g| \gg |\zeta_i|, \quad |\nabla_s\zeta_g| \gg |\nabla_s\zeta_i|. \tag{2.8}$$

The first two inequalities describe the fact that for internal-wave motion there is little displacement of the ocean surface. The third inequality states that the surface slope due to internal waves is expected to be much less than that due to surface waves.

To describe the surface-wave motion, we define the high frequency velocity potential on the surface $z = \zeta_t(\mathbf{r}, t)$ as

$$\phi_s(\mathbf{r}, t) \equiv \phi_g(\mathbf{r}, \zeta_t(\mathbf{r}, t), t). \tag{2.9}$$

With use of the inequalities (2.8), we extract the high frequency, short wavelength part from (2.3) to obtain the coupled equations

$$(\partial/\partial t + \mathbf{U}.\nabla_s)\,\phi_s + g\zeta_g = 0, \tag{2.10a}$$

$$(\partial\zeta_g/\partial t) + \nabla_s.(\mathbf{U}\zeta_g) = \kappa\phi_s. \tag{2.10b}$$

In deriving (2.10) we have used Laplace's equation to eliminate the vertical derivative and in so doing have introduced the operator

$$\kappa \equiv (-\nabla_s^2)^{\frac{1}{2}}. \tag{2.11}$$

It is understood that κ will always act on a Fourier series. To illustrate this, we write

$$\phi_s = \Sigma\beta(\mathbf{k}) \exp(i\mathbf{k}.\mathbf{r}),$$

then

$$\kappa\phi_s \equiv \sum_{\mathbf{k}} k\beta(\mathbf{k}) \exp(i\mathbf{k}.\mathbf{r}).$$

In deriving (2.10) we have also neglected nonlinear terms which do not couple surface and internal waves. In (2.10*a*) we have neglected terms $O(w_s|\nabla_s\phi_s|)$ and smaller. Similarly, in (2.10*b*) we have neglected terms $O(|\dot{\zeta}_g\dot{U}|/g)$ and smaller, where $\partial U/\partial t \equiv \dot{U}$, etc.

We next extract the low frequency, long wavelength part of (2.3). On following an argument of Phillips [1966, equation (5.2.12)], we obtain with a little straightforward algebra the surface boundary condition

$$[\partial\phi_i/\partial z]_{z=0} = \nabla_s.\langle\zeta_g\nabla_s\phi_s\rangle_{FL} \equiv \Gamma(\mathbf{r}, t). \tag{2.12}$$

Here we have written $\langle F\rangle_{LF}$ as representing the 'low frequency, long wavelength part' of the quantity F. On taking account of a cancellation of certain terms, we find that the largest terms neglected in (2.12) are of relative order (internal-wave frequency/surface-wave frequency).

The linearized form of (2.4), i.e. $Q = 0$, (2.10) and the boundary condition (2.12) are the equations used in this paper to study surface-wave/internal-wave interactions. If the nonlinear couplings were neglected, (2.10) would describe linearized surface waves. Similarly, (2.12) would be replaced by

$$[\partial\phi_i/\partial z]_{z=0} = 0, \tag{2.13}$$

which together with the linearized form of (2.4) describes linear internal wave modes.

We now re-express (2.4), (2.10) and (2.13) as rate equations for the time evolution of the linear mode amplitudes. In the absence of coupling between the surface and internal waves, the general solution to (2.10) can be expanded in a Fourier series, within the rectangular area of ocean being considered, as

$$\phi_s(\mathbf{r}, t) = \sum_{\mathbf{k}} C(\mathbf{k}) \exp(i\mathbf{k}.\mathbf{r}), \tag{2.14a}$$

$$\zeta_g(\mathbf{r}, t) = (i/g) \sum_{\mathbf{k}} \omega_k C(\mathbf{k}) \exp(i\mathbf{k}.\mathbf{r}). \tag{2.14b}$$

Here $\omega_k = (gk)^{\frac{1}{2}}$ and the Fourier amplitudes $C(\mathbf{k})$ satisfy the equation

$$\ddot{C}(\mathbf{k}) + \omega_k^2 C(\mathbf{k}) = 0. \tag{2.15}$$

The vertical velocity for linear internal waves may similarly be expanded in the form

$$w(\mathbf{r}, z, t) = \sum_{j,\mathbf{K}} A_{j,\mathbf{K}}(t)\, W_{j,K}(z) \exp(i\mathbf{K}.\mathbf{r}), \tag{2.16}$$

where $(j, \mathbf{K})$ describes an internal wave of vertical mode number j ($j = 1, 2, \ldots$, in the notation of Garrett & Munk 1972*a*) and horizontal wave vector $\mathbf{K}$. Also, in the absence of coupling the coefficients $A_{j,\mathbf{K}}$ satisfy the equation

$$\ddot{A}_{j,\mathbf{K}} + \Omega^2(j, K) A_{j,\mathbf{K}} = 0. \tag{2.17}$$

Substitution of the expansion (2.16) into (2.4), with $Q = 0$, gives the equation (here $W' \equiv dW/dz$, etc.)

$$W''_{j,K} + K^2[N^2/\Omega^2(j, K) - 1]\, W_{j,K} = 0. \tag{2.18}$$

The boundary condition (2.13), which applies in the absence of nonlinear coupling, and that at $z = -B$ imply that

$$W_{j,K}(0) = W_{j,K}(-B) = 0. \tag{2.19}$$

The normalization of $W_{j,K}$ is so chosen that in the mixed layer, where $N = 0$,

$$W_{j,K} = K \sinh(Kz), \quad -D < z < 0. \tag{2.20}$$

The expressions (2.16) and (2.20) permit us to write the velocity potential ϕ_i at the surface $z = 0$ as

$$\phi_i(\mathbf{r}, 0, t) = \sum_{j,\mathbf{K}} A_{j,\mathbf{K}}(t) \exp(i\mathbf{K}.\mathbf{r}). \tag{2.21}$$

The vertical displacement $\Xi(\mathbf{r}, t)$ at the pycnocline will be used as a convenient indicator of the internal-wave amplitude. This is written as

$$\Xi = \sum_j \xi_j(\mathbf{r}, t),$$

$$\partial \xi_j/\partial t = \sum_{\mathbf{K}} A_{j,\mathbf{K}}(t)\, W_{j,K}(-D) \exp(i\mathbf{K}.\mathbf{r}). \tag{2.22}$$

The nonlinear interaction of surface and internal waves modifies (2.15) and (2.17). This modification describes an exchange of energy among the linear modes. For our application the time scale for this nonlinear exchange, say t_{NL}, is characteristically large compared with the linear wave periods. We therefore assume (and later justify) that

$$t_{NL}\, \Omega(j, K) \gg 1, \quad t_{NL}\, \omega_k \gg 1 \tag{2.23}$$

for wavenumbers and mode numbers of interest here.

The modified form of (2.15) is readily obtained from (2.10) by using (2.21) to calculate the fluid velocity $\mathbf{U} = \nabla_s \phi_i$ and again expanding ζ_g and ϕ_s in the linear modes of (2.14). The resulting equations are of the form

$$\ddot{C}(\mathbf{k}) + \omega_k^2 C(\mathbf{k}) = [\nabla_s.(\mathbf{U}\zeta_g) - \partial(\mathbf{U}.\nabla_s \phi_s)/\partial t]_{\mathbf{k}}, \tag{2.24}$$

where $[\ldots]_{\mathbf{k}}$ implies the Fourier amplitude of the quantity in square brackets.

To modify (2.17) also so as to include the nonlinear couplings, we must use the boundary condition (2.12). The modification requires that we rewrite (2.16) in the form

$$w(\mathbf{r},z,t) = \sum_{\mathbf{K}} [\sum_{j} A_{j,\mathbf{K}}(t)\, W_{j,K}(z) + \Delta W_{\mathbf{K}}(z)] \exp(i\mathbf{K}.\mathbf{r}). \tag{2.25}$$

The term $\Delta W_{\mathbf{K}}$ is required to satisfy the boundary condition (2.12), which is written as

$$\Delta W_{\mathbf{K}}(0) = \Gamma_{\mathbf{K}}(t), \tag{2.26}$$

where $\Gamma_{\mathbf{K}}(t)$ is the Fourier amplitude corresponding to a wave vector $\mathbf{K}$ of $\Gamma(\mathbf{r},t)$.

If we substitute (2.25) into (2.4) and use (2.18), we obtain the equation

$$\sum_{j} [\ddot{A}_{j,\mathbf{K}} + \Omega^2(j,K)\, A_{j,\mathbf{K}}]\, \Omega^{-2}(j,K)\, K^2 N^2 W_{j,K} - \left[\frac{\partial^2}{\partial t^2}\left(\frac{\partial^2}{\partial z^2} - K^2\right) - N^2K^2\right] \Delta W_{\mathbf{K}} = 0. \tag{2.27}$$

To simplify this equation further we multiply by $W_{n,K}$ and integrate with respect to z. The orthogonality relation

$$\int_{-B}^{0} N^2 W_{n,K}\, W_{j,K}\, dz = 0 \quad \text{if} \quad n \neq j$$

permits us to write

$$[\ddot{A}_{j,\mathbf{K}}\, \Omega^{-2}(j,K) + A_{j,\mathbf{K}}]\, K^2 \int_{-B}^{0} N^2 (W_{j,K})^2\, dz = \int_{-B}^{0} dz W_{j,K} \left[\frac{\partial^2}{\partial t^2}\left(\frac{\partial^2}{\partial z^2} - K^2\right) - N^2K^2\right] \Delta W_{\mathbf{K}}. \tag{2.28}$$

In the absence of nonlinear coupling, we should have $\Delta W_{\mathbf{K}} = 0$ and solutions of the form

$$A_{j,\mathbf{K}}(t) = A_{j,\mathbf{K}}(0) \exp[i\Omega(j,K)\, t]$$

would result. The effect of the nonlinear coupling is anticipated to lead to a variation of the $A_{j,\mathbf{K}}(0)$'s on the time scale t_{NL}.

The nonlinear term on the right-hand side of (2.28) will be of importance in our calculations only for the frequency components of $\Delta W_{\mathbf{K}}$ which closely match those of $A_{j,\mathbf{K}}$ (the 'resonance condition'). We are therefore justified in replacing $\partial^2/\partial t^2$ by $[-\Omega^2(j,K)]$ in the right-hand side of (2.28)†. Use of (2.18) then leads immediately to the equation

$$\ddot{A}_{j,\mathbf{K}} + \Omega^2(j,K)\, A_{j,\mathbf{K}} = \Omega^4(j,K)\, W'_{j,K}(0)\, \Gamma_{\mathbf{K}} \left[K^2 \int_{-B}^{0} N^2 (W_{j,K})^2\, dz\right]^{-1}, \tag{2.29}$$

where (2.26) has been used.

For subsequent calculations we define a quantity $g'(j,K)$ by the equation

$$\int_{-B}^{0} N^2 (W_{j,K})^2\, dz \equiv g'(j,K)\, W^2_{j,K}(-D) = K^2 \sinh^2(KD)\, g'(j,K). \tag{2.30}$$

† A more formal way to obtain this result would be to introduce 'fast' and 'slow' time scales. Multiplication of (2.28) by $\exp[i\Omega(j,K)\, t]$ and averaging over the fast time scale would then lead to (2.29). (Compare Whitham 1974, chap. 14.)

The quantity $\Gamma_{\mathbf{K}}$ is expressed in terms of the surface-wave amplitudes using (2.12) and $W'_{j,K}(0) = K^2$ from (2.20).

Equations (2.24) and (2.29) represent the coupled dynamic equations which we shall use to describe the interaction of surface and internal waves. Our experience with numerical integration of such equations leads us to replace the mode amplitudes $C(\mathbf{k})$ and $A_{j,\mathbf{K}}$ by classical action–angle variables $J(\mathbf{k})$, $\Theta(\mathbf{k})$, $J(j,\mathbf{K})$ and $\Theta(j,\mathbf{K})$. The resulting equations replacing (2.24) and (2.29) are of first order in time and are very stable when integrated numerically. The surface mode amplitudes in terms of action and angle variables are

$$C(\mathbf{k}) = [gJ(\mathbf{k})/(2\rho_0\omega_k)]^{\frac{1}{2}} \exp[\pm i\Theta(\mathbf{k})] \tag{2.31a}$$

and the internal mode amplitudes are

$$A_{j,\mathbf{K}} = \{\Omega(j,K)\,J(j,\mathbf{K})/[\rho_0 T(j,K)]\}^{\frac{1}{2}} \exp[\pm i\Theta(j,\mathbf{K})], \tag{2.31b}$$

where

$$T(j,K) \equiv [g'(j,K)]^{\frac{1}{2}} K \sinh(KD)/\Omega(j,K). \tag{2.32}$$

Travelling waves or standing waves may be constructed by inserting (2.31) into (2.14) and (2.21). For the calculations described in the following sections, travelling waves with periodic boundary conditions were employed. The expressions for the velocity potentials and displacements then have the form

$$\phi_s(\mathbf{r},t) = \sum_{\mathbf{k}} \left[\frac{2gJ(\mathbf{k})}{\rho_0\omega_k}\right]^{\frac{1}{2}} \cos[\mathbf{k}.\mathbf{r} - \Theta(\mathbf{k})], \tag{2.33a}$$

$$\zeta_g(\mathbf{r},t) = -\sum_{\mathbf{k}} \left[\frac{2\omega_k J(\mathbf{k})}{\rho_0 g}\right]^{\frac{1}{2}} \sin[\mathbf{k}.\mathbf{r} - \Theta(\mathbf{k})], \tag{2.33b}$$

for the surface waves. For the internal waves the corresponding relations are

$$\phi_i(\mathbf{r},0,t) = \sum_j \phi_j(\mathbf{r},t), \tag{2.34a}$$

$$\phi_j(\mathbf{r},t) = \sum_{\mathbf{K}} \left[\frac{2\Omega(j,K)\,J(j,\mathbf{K})}{\rho_0 T(j,K)}\right]^{\frac{1}{2}} \cos[\mathbf{K}.\mathbf{r} - \Theta(j,\mathbf{K})], \tag{2.34b}$$

$$\xi_j(\mathbf{r},t) = \sum_{\mathbf{K}} \left[\frac{2\Omega(j,K)\,J(j,\mathbf{K})}{\rho_0 g'(j,K)}\right]^{\frac{1}{2}} \sin[\mathbf{K}.\mathbf{r} - \Theta(j,\mathbf{K})]. \tag{2.34c}$$

The equations of motion in terms of the action–angle variables can be obtained by directly substituting (2.31*a*) in (2.24) and (2.31*b*) in (2.29). The surface current $\mathbf{U}$ in (2.24) must then be expressed in action angle variables using (2.31*b*) in (2.21), and the low frequency surface gravity waves in $\Gamma_{\mathbf{k}}$ must be expressed in action–angle variables using (2.31*a*). This lengthy algebraic procedure results in a system of coupled second-order differential equations which must be numerically integrated for the physical problems of interest. An alternative method which yields a coupled system of *first*-order differential equations is to construct a Hamiltonian H for the coupled surface-wave/internal-wave system from which the equations of motion immediately follow using Hamilton's equations (see

Watson, West & Cohen 1975). The proper Hamiltonian for the coupled system is

$$H = H_s + H_I + V, \tag{2.35}$$

where
$$H_s = \sum_{\mathbf{k}} J(\mathbf{k})\,\omega_k, \quad H_I = \sum_{j,\mathbf{K}} J(j,\mathbf{K})\,\Omega(j,K), \tag{2.36a, b}$$

$$V = -\sum_{\substack{\mathbf{k},\mathbf{n}\\ j,\mathbf{K}}} \delta_{\mathbf{k}-\mathbf{n}-\mathbf{K}} G(\mathbf{k},\mathbf{n};j,\mathbf{K})\,[J(\mathbf{k})J(\mathbf{n})J(j,\mathbf{K})]^{\frac{1}{2}} \sin[\Theta(\mathbf{k})-\Theta(\mathbf{n})-\Theta(j,\mathbf{K})]. \tag{2.36c}$$

The quantities H_s and H_I represent, respectively, the energy per unit area for freely propagating surface and internal waves. The effect of surface-wave/internal-wave coupling, as given in (2.24) and (2.29), is described by the term V in (2.36). For brevity we shall not describe the derivation of these expressions here. Their validity may be directly verified, however, by comparing Hamilton's equations (2.37) with (2.24) and (2.29).

The equations of motion in terms of the action–angle variables are

$$\dot{J}(\mathbf{k}) = -\frac{\partial H}{\partial \Theta(\mathbf{k})} = \sum_{j,\mathbf{K}} 2\{\hat{G}(\mathbf{k},j,\mathbf{K})\,[J(\mathbf{k})J(\mathbf{k}-\mathbf{K})J(j,\mathbf{K})]^{\frac{1}{2}} \cos\psi(\mathbf{k},j,\mathbf{K}) - \hat{G}(\mathbf{k}+\mathbf{K},j,\mathbf{K})\,[J(\mathbf{k}+\mathbf{K})J(\mathbf{k})J(j,\mathbf{K})]^{\frac{1}{2}} \cos\psi(\mathbf{k}+\mathbf{K},j,\mathbf{K})\}, \tag{2.37a}$$

$$\dot{J}(j,\mathbf{K}) = -\frac{\partial H}{\partial \Theta(j,\mathbf{k})} = -\sum_{\mathbf{k}} 2\hat{G}(\mathbf{k},j,\mathbf{K})\,[J(\mathbf{k})J(\mathbf{k}-\mathbf{K})J(j,\mathbf{K})]^{\frac{1}{2}} \cos\psi(\mathbf{k},j,\mathbf{K}), \tag{2.37b}$$

$$\begin{aligned}\dot{\psi}(\mathbf{k},j,\mathbf{K}) = {} & \frac{\partial H}{\partial J(\mathbf{k})} - \frac{\partial H}{\partial J(\mathbf{k}-\mathbf{K})} - \frac{\partial H}{\partial J(j,\mathbf{K})} = \omega_k - \omega_{|\mathbf{k}-\mathbf{K}|} - \Omega(j,K) \\ & - \sum_{j',\mathbf{M}} \hat{G}\{(\mathbf{k},j',\mathbf{M})\,[J(\mathbf{k}-\mathbf{M})J(j',\mathbf{M})/J(\mathbf{k})]^{\frac{1}{2}} \sin\psi(\mathbf{k},j',\mathbf{M}) \\ & + \hat{G}(\mathbf{k}+\mathbf{M},j',\mathbf{M})\,[J(\mathbf{k}+\mathbf{M})J(j',\mathbf{M})/J(\mathbf{k})]^{\frac{1}{2}} \sin\psi(\mathbf{k}+\mathbf{M},j',\mathbf{M}) \\ & - \hat{G}(\mathbf{k}-\mathbf{K},j',\mathbf{M})\,[J(\mathbf{k}-\mathbf{K}-\mathbf{M})J(j',\mathbf{M})/J(\mathbf{k}-\mathbf{K})]^{\frac{1}{2}} \sin\psi(\mathbf{k}-\mathbf{K},j',\mathbf{M}) \\ & - \hat{G}(\mathbf{k}-\mathbf{K}+\mathbf{M},j',\mathbf{M})\,[J(\mathbf{k}-\mathbf{K}+\mathbf{M})J(j',\mathbf{M})/J(\mathbf{k}-\mathbf{K})]^{\frac{1}{2}} \sin\psi(\mathbf{k}-\mathbf{K}+\mathbf{M},j',\mathbf{M})\} \\ & + \sum_{\mathbf{p}} \hat{G}(\mathbf{p},j,\mathbf{K})\,[J(\mathbf{p})J(\mathbf{p}-\mathbf{K})/J(j,\mathbf{K})]^{\frac{1}{2}} \sin\psi(\mathbf{p},j,\mathbf{K}),\end{aligned} \tag{2.37c}$$

where the angle variables always occur in the combination

$$\psi(\mathbf{k},j,\mathbf{K}) \equiv \Theta(\mathbf{k}) - \Theta(\mathbf{k}-\mathbf{K}) - \Theta(j,\mathbf{K}). \tag{2.38}$$

In these equations we have written

$$\hat{G}(\mathbf{k},j,\mathbf{K}) \equiv G(\mathbf{k},\mathbf{k}-\mathbf{K};j,\mathbf{K})$$

and
$$G(\mathbf{k},\mathbf{n};j,\mathbf{K}) = \mathbf{K}.[\omega_n\mathbf{k}+\omega_k\mathbf{n}]\,[\Omega(j,K)/(\omega_n\omega_k\rho_0 8)]^{\frac{1}{2}}/T(j,K). \tag{2.39}$$

In writing (2.36) and (2.37) we have dropped as unimportant some rapidly oscillating terms involving $\sin[\Theta(\mathbf{k})+\Theta(\mathbf{n})+\Theta(j,\mathbf{K})]$.

In the absence of nonlinear coupling, the actions $J(\mathbf{k})$ and $J(j,\mathbf{K})$ are constant and $\Theta(\mathbf{k}) = \omega_k t$ + initial value, $\Theta(j,\mathbf{K}) = \Omega(j,\mathbf{K})\,t$ + initial value, as is clear from (2.37). We see then from (2.33) and (2.34) that our choice of variables is such that each linear mode corresponds to a progressive wave with wave vectors $\mathbf{k}$, $\mathbf{K}$, etc.

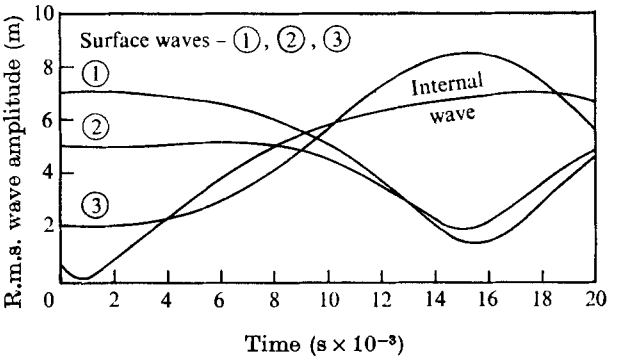

FIGURE 1. The r.m.s. amplitudes for three surface- and one internal-wave mode are shown as functions of time.

[The expansions (2.33) and (2.34) may easily be modified to describe standing waves.]

The practicality of the equations of motion (2.37) is demonstrable in that integration of the coupled, first-order, ordinary differential equations has been achieved numerically to high accuracy with the simplest, first-order Euler scheme.

We describe a numerical integration of (2.37) for a simple example chosen to illustrate time scales and frequency resonance. For this calculation we take $D = 100$ m and $\delta\rho/\rho_0 = 10^{-3}$ and use the two-layer model of (1.3). A single internal-wave mode of wave vector $\mathbf{K}$ interacts with three surface-wave modes of respective wave vectors

$$\mathbf{k}_1,\ \mathbf{k}_2 = \mathbf{k}_1 - \mathbf{K},\ \mathbf{k}_3 = \mathbf{k}_1 - 2\mathbf{K}. \tag{2.40}$$

The phases $\psi(\mathbf{k}, j, \mathbf{K})$, at time $t = 0$, are all set equal to zero in (2.37).

We choose the modes with wave vectors in polar co-ordinates $k_1 = (0{\cdot}03\ \mathrm{m}^{-1}, 0°)$, $k_2 = (0{\cdot}029896\ \mathrm{m}^{-1}, 1{\cdot}9°)$, $k_3 = (0{\cdot}029824\ \mathrm{m}^{-1}, -3{\cdot}8°)$ and $K = (0{\cdot}001\ \mathrm{m}^{-1}, 83°)$ and with frequency differences $\Delta\omega_{12} = 9{\cdot}44 \times 10^{-4}\ \mathrm{s}^{-1}$, $\Delta\omega_{13} = 1{\cdot}59 \times 10^{-3}\ \mathrm{s}^{-1}$ and $\Delta\omega_{23} = 6{\cdot}48 \times 10^{-4}\ \mathrm{s}^{-1}$, with $\Delta\omega_{ij} \equiv \omega_i - \omega_j$. The root-mean-square (r.m.s.) amplitudes of the four modes, i.e. $\langle\zeta_g^2\rangle^{\frac{1}{2}}$ or $\langle\zeta_i^2\rangle^{\frac{1}{2}}$, are shown in figure 1 as a function of time. The initial decrease in amplitude of the internal-wave mode is a consequence of our choice of initial condition that the phases ψ vanish at $t = 0$. As $J(1, \mathbf{K})$ reaches its minimum value, the phase $\psi(\mathbf{k}, 1, \mathbf{K})$ switches to the value π, and $J(1, \mathbf{K})$ begins to increase. Note that $\Delta\omega_{12} = \Omega(1, K)$, thereby forming a resonant triad and that $\Delta\omega_{23}$ is close enough to resonance that significant coupling to mode 3 occurs after the mode 2 amplitude has reached about 4 m. For a slightly different value of $\Delta\omega_{23}$ it was found that the amplitude of wave 3 remained constant throughout the interaction, i.e. no energy exchange.

This example suggests the following generalization. If we write

$$\mathbf{k}_n = \mathbf{k}_1 - (n-1)\mathbf{K}, \quad n = 2, 3, \ldots, \tag{2.41}$$

and assume $k_1 \gg nK$ for n's considered, then with $\omega_n \equiv \omega_{\mathbf{k}_n}$

$$\omega_{n-1} - \omega_n \cong \mathbf{K}.\mathbf{C}(\mathbf{k}_1),$$

where $\mathbf{C}(\mathbf{k}_1)$ is the group velocity of mode 1. Now if

$$\Omega(1, K) \cong \mathbf{K}.\mathbf{C}(\mathbf{k}_1), \tag{2.42}$$

we satisfy the resonance condition between the internal wave and adjacent pairs of surface waves. In this case, a 'cascade' process of energy exchange can result, just as has been noted for laser–plasma wave couplings (see Cohen, Kaufman & Watson 1972).

3. Applications to ocean waves

In this section we relate the formalism developed in §2 to ocean wave phenomena and discuss some consequences of (2.37).

The power spectrum $\Psi_s(\mathbf{k})$ of ocean surface waves has been reviewed by Phillips (1966, §4.1). This spectrum is so normalized that

$$\sum_{\mathbf{k}} \frac{(2\pi)^2}{A_0} \Psi_s(\mathbf{k}) \to \int d^2k \Psi_s(\mathbf{k}) = \langle \zeta_g^2 \rangle. \tag{3.1}$$

Here the angular brackets represent an ensemble average over many specific realizations of the ocean. For simplicity, we assume that $\langle \zeta_g^2 \rangle$ is independent of position on the ocean surface. In writing (3.1) we have replaced a sum over discrete modes in the surface region of area A_0 by an integral over wavenumber.

The corresponding internal-wave power spectrum $\Psi_I(j, \mathbf{K})$ has been discussed by Garrett & Munk (1972*a*, 1975). The indicated arguments of Ψ_I are the mode number j and wavenumber $\mathbf{K}$. This spectrum is so normalized that

$$\sum_{j=1}^{\infty} \int d^2K \Psi_I(j, \mathbf{K}) = \sum_{j=1}^{\infty} \langle \xi_j^2 \rangle = \langle \Xi^2 \rangle, \tag{3.2}$$

which is here considered to be independent of $\mathbf{r} = (x, y)$ and to be evaluated at $z = -D$, the pycnocline depth.

These power spectra may be related to the action variables using (2.33) and (2.34). We first observe that

$$\langle \zeta_g^2 \rangle = \sum_{\mathbf{k}} \langle J(\mathbf{k}) \omega_k \rangle / (g\rho_0),$$

$$\langle \xi_j^2 \rangle = \sum_{\mathbf{k}} \langle J(j, \mathbf{K}) \Omega(j, K) \rangle / [\rho_0 g'(j, K)].$$

Therefore, using (3.1) and (3.2) we obtain

$$\langle J(\mathbf{k}) \rangle = [(2\pi)^2 g\rho_0 / (\omega_k A_0)] \Psi_s(\mathbf{k}), \tag{3.3a}$$

$$\langle J(j, \mathbf{K}) \rangle = [(2\pi)^2 g'(j, K) \rho_0 / (\Omega(j, K) A_0)] \Psi_I(j, \mathbf{K}). \tag{3.3b}$$

The equilibrium surface-wave spectrum suggested by Phillips (1966, §45) is of the form

$$\Psi_s(\mathbf{k}) = 4 \times 10^{-3} k^{-4} \mathscr{G}_s(k, \beta) h(k), \quad k_s > k > k_0, \tag{3.4a}$$

$$h(k) = \begin{cases} 1 & \text{for} \quad k_s > k > k_0, \\ 0 & \text{for} \quad k < k_0 \quad \text{or} \quad k > k_s. \end{cases} \tag{3.4b, c}$$

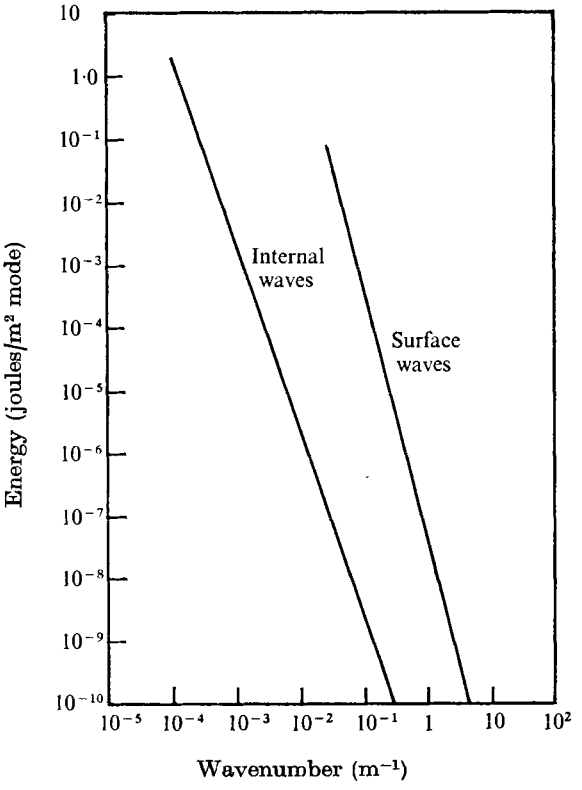

FIGURE 2. The energy per mode for surface and internal waves is shown as a function of a wavenumber. The equilibrium spectra of Phillips (1966) and Garrett & Munk (1975) with $D = 100$ m and $\delta\rho/\rho_0 = 10^{-3}$ are used.

Phillips chose

$$\mathscr{G}_s(k,\beta) = \begin{cases} \pi^{-1} & \text{for } \hat{\mathbf{k}}.\hat{\mathbf{w}} \equiv \cos\beta > 0, \quad (3.5a) \\ 0 & \text{for } \hat{\mathbf{k}}.\hat{\mathbf{w}} < 0, \quad (3.5b) \end{cases}$$

where $\hat{\mathbf{w}}$ is a unit vector in the direction the wind is blowing. The internal-wave spectrum suggested by Garrett & Munk (1975) is

$$\Psi_I(j,\mathbf{K}) = 8{\cdot}5\times10^{-4}Kj/[(K^2+1{\cdot}15\times10^{-3}j^2)^2(j^2+9)]. \quad (3.6)$$

The energy per mode per unit area, $\langle\omega_k J(\mathbf{k})\rangle$ and $\langle\Omega(1,K)J(1,\mathbf{K})\rangle$, is shown in figure 2 as a function of wavenumber, using (3.3), (3.4) and (3.6). We assume a 'rectangular ocean' of dimensions 100×100 km and use the Garrett–Munk frequency profile (1.2) with $D = 100$ m and $\delta\rho/\rho_0 = 10^{-3}$.

We next study the transfer of excitation from a sharply collimated spectrum of surface waves to internal waves, using the Garrett–Munk ocean model (1.2). By 'sharply collimated', we mean that the function $\mathscr{G}_s(k,\beta)$ in (3.4) vanishes unless $\beta \cong \beta_0$, a constant. The excitation of a single internal-wave mode $(j,\mathbf{K})$ having a very small action variable $J(j,\mathbf{K})$ will be considered. The energy source

for driving this internal-wave mode will be a set of large amplitude surface waves having wave vectors $\mathbf{p}_1, \mathbf{p}_2, \ldots$ and corresponding action variables

$$J^0(\mathbf{p}_1), J^0(\mathbf{p}_2), \ldots .$$

The set of waves consisting of the third members of resonant triads are surface waves of small amplitude having wave vectors $\mathbf{k}_i = \mathbf{p}_i - \mathbf{K}$ and respective action variables $J(\mathbf{k}_i)$ $(i = 1, 2, \ldots)$. We shall assume that the large amplitude quantities $J^0(\mathbf{p}_i)$ are constant during the time of interaction (the approximation of *parametric amplification*; see, for example, Nishikawa 1968). The 'locked phase' approximation in which the relative phases of the modes are assumed constant in time will also be used, so (2.37) now reads

$$\dot{J}(\mathbf{k}_i) = 2\hat{G}(\mathbf{p}_i, j, \mathbf{K})\,[J^0(\mathbf{p}_i)\,J(\mathbf{k}_i)\,J(j, \mathbf{K})]^{\frac{1}{2}}, \tag{3.7a}$$

$$\dot{J}(j, \mathbf{K}) = \sum_i 2\hat{G}(\mathbf{p}_i, j, \mathbf{K})\,[J^0(\mathbf{p}_i)\,J(\mathbf{k}_i)\,J(j, \mathbf{K})]^{\frac{1}{2}}, \tag{3.7b}$$

and $\cos\psi(\mathbf{p}_i, j, \mathbf{K}) = -1$ for all modes (assumed).

We look for a solution to (3.7) of the form

$$J(\mathbf{k}_i) = C_i \exp(\alpha t), \quad J(j, \mathbf{K}) = D \exp(\alpha t) \tag{3.8}$$

and find that

$$\alpha^2(j, K) = \sum_i [2\hat{G}(\mathbf{p}_i, j, \mathbf{K})]^2 J^0(\mathbf{p}_i).$$

Using (3.3a) and transforming from the discrete to the continuous system we can re-express α^2 as an integral over the surface-wave spectrum:

$$\alpha^2(j, K) = \int d^2k 4g\rho_0 [\hat{G}(\mathbf{k}, j, \mathbf{K})]^2 \Psi_s(\mathbf{k})/\omega_k. \tag{3.9}$$

To simplify (3.9) we use the assumed condition that $K \ll k$ and (2.39) to write

$$[\hat{G}(\mathbf{k}, j, \mathbf{K})]^2 \cong \frac{\Omega(j, K)}{2\rho_0 T^2(j, K)} (\mathbf{k}.\mathbf{K} - \tfrac{1}{2}K^2)^2.$$

Now the resonance condition

$$f = \omega_{|\mathbf{k}-\mathbf{K}|}, \quad f \equiv \omega_k - \Omega(j, K), \tag{3.10}$$

lets us write

$$(\mathbf{k}.\mathbf{K} - \tfrac{1}{2}K^2)^2 \cong 4k^3\Omega^2(j, K)/g. \tag{3.11}$$

Collecting these results, and using the spectral representations (3.4), we can write (3.9) in the form

$$\alpha^2(j, K) = \frac{3{\cdot}2 \times 10^{-2}\Omega^5(j, K)}{g'(j, K)\,K^2 \sinh^2(KD)} \int \frac{dk}{\omega_k} h(k) \int d\beta \mathscr{G}_s(k, \beta). \tag{3.12}$$

The observations of Tyler *et al.* (1974) suggest that the spectral angular distribution $\mathscr{G}_s(k, \beta)$ in (3.4) is strongly peaked near the long wavelength cut-off k_0 and in the direction the wind is blowing. If a modification of the Phillips spectrum (3.4) is desired (for example, to describe a swell) an appropriate function $h(k)$ may be used in (3.12).

Now, (3.13) implies that, for $k \approx k_0$, $\mathbf{k}$ and $\mathbf{K}$ are nearly perpendicular, so we might anticipate that a well collimated beam of surface waves would generate internal waves propagating at nearly right-angles to the direction of the surface

$\delta\rho/\rho_0 = 0$				$\delta\rho/\rho_0 = 3\times10^{-4}$			
Mode number	Wave-number (m^{-1}) K	Angular frequency (rad/s) $\Omega(j, K)$	WKB turning depth (m)	Mode number j	Wave-number (m^{-1}) K	Angular frequency (rad/s) $\Omega(j, K)$	WKB turning depth (m)
1	10^{-3}	$2{\cdot}0\times10^{-3}$	1230	1	10^{-3}	$2{\cdot}0\times10^{-3}$	1220
1	3×10^{-3}	$3{\cdot}8\times10^{-3}$	490	1	3×10^{-3}	$3{\cdot}8\times10^{-3}$	480
1	10^{-2}	$4{\cdot}9\times10^{-3}$	165	1	10^{-2}	$5{\cdot}1\times10^{-3}$	130
2	10^{-3}	$1{\cdot}0\times10^{-3}$	2030	2	10^{-3}	$1{\cdot}1\times10^{-3}$	2000
2	3×10^{-3}	$2{\cdot}4\times10^{-3}$	1030	2	3×10^{-3}	$2{\cdot}5\times10^{-3}$	990
2	10^{-2}	$4{\cdot}2\times10^{-3}$	360	2	10^{-2}	$4{\cdot}5\times10^{-3}$	270

TABLE 1. Internal-wave angular frequencies and WKB turning-point depths are listed for modes 1 and 2 and several wavenumbers. The Garrett–Munk ocean model (1.2) is used in the calculation.

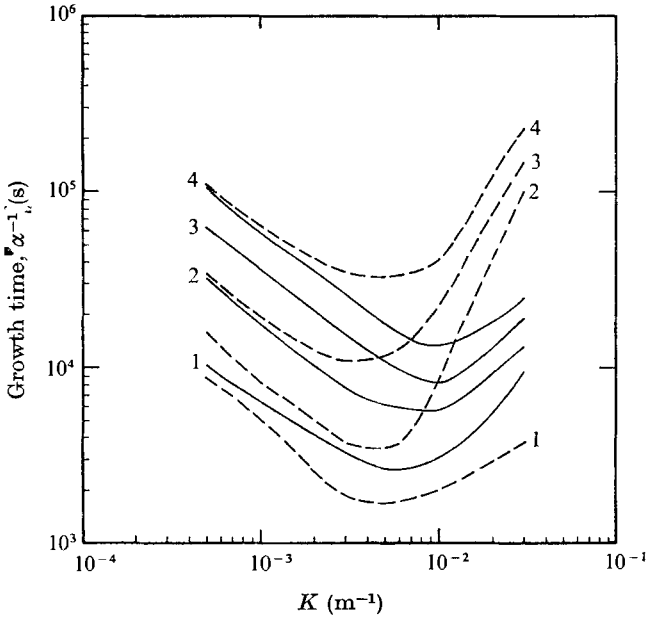

FIGURE 3. The e-folding time for growth of an internal wave of wavenumber K due to large amplitude swell is shown. Growth times are shown for the four lowest modes ($j = 1, 2, 3, 4$) and a mixed-layer thickness of 100 m. ———, $\delta\rho/\rho_0 = 0$; – – – –, $\delta\rho/\rho_0 = 10^{-3}$.

waves (Hasselmann 1966; Kenyon 1968). Apel *et al.* (1975*a*) have, indeed, reported what seem to be internal waves generated by a large swell and propagating at nearly right-angles to the swell.

To model this phenomenon, we take $\mathscr{G}_s(k, \beta) = \delta(\beta)$ and evaluate the integral in (3.12) as

$$\int \frac{dk}{\omega_k} h(k) \int d\beta \mathscr{G}_s(k, \beta) \equiv \frac{1}{V_c}, \tag{3.13}$$

where V_c is a 'characteristic velocity'.

To complete the numerical evaluation of the growth rate α from (3.12) we use the Garrett–Munk ocean model (1.2). The internal-wave eigenmodes are evaluated from (2.16) and (2.17) using the WKB approximation, and the coupling coefficients g' are then calculated using (2.30). Some illustrative results are given in table 1 for the angular frequency Ω and the WKB turning-point depth.

For the choice $V_c = 20$ m/s† we have displayed the growth rate $\alpha^{-1}(j, K)$ (in seconds) as a function of wavenumber K in figure 3 for the first four modes, corresponding to $j = 1, 2, 3, 4$. The mixed-layer depth D is here 100 m. The solid curves correspond to $\delta\rho/\rho_0 = 0$, the dashed curves to $\delta\rho/\rho_0 = 10^{-3}$ at the pycnocline. The lowest-order internal-wave modes are excited much more strongly than are the higher modes. Since the lower modes are concentrated nearer the ocean surface this is not unexpected. We stress that the variation in density at the pycnocline is superimposed on the more general frequency profile given by (1.2).

Some insight into the validity of the 'locked phase' and 'parametric amplification' approximation will be found in the next section, where the numerical integration of (2.37) is studied.

4. Generation of internal waves from an equilibrium surface spectrum

In this section we study the generation of a specific internal-wave mode $(j, \mathbf{K})$ by an equilibrium surface-wave spectrum. For this we use the expression (3.4) with $\mathscr{G}_s(k, \beta)$ given by (3.5). Since the spectrum (3.4) is isotropic over a hemisphere, the generated internal-wave spectrum will be approximately isotropic. A set of interacting triads will have surface wavenumbers $\mathbf{p}_i$ and $\mathbf{k}_i = \mathbf{p}_i - \mathbf{K}$, $i = 1, 2, \ldots$.

To simplify the notation, we write $\Omega \equiv \Omega(j, K)$, $G_i \equiv \hat{G}(\mathbf{p}_i, j, \mathbf{K})$, $\psi_i \equiv \psi(\mathbf{p}_i, j, \mathbf{K})$ and $\mathscr{J} \equiv J(j, \mathbf{K})$. Then, for the set of interacting triads, (2.37) can be written in the form

$$\dot{J}(\mathbf{k}_i) = -2G_i[J(\mathbf{p}_i)\,J(\mathbf{k}_i)\,\mathscr{J}]^{\frac{1}{2}}\cos\psi_i = -\dot{J}(\mathbf{p}_i), \tag{4.1a}$$

$$\dot{\mathscr{J}} = \sum_i \dot{J}(\mathbf{k}_i), \tag{4.1b}$$

$$\dot{\psi}_i = \omega_{p_i} - \omega_{k_i} - \Omega + \sum_n G_n[J(\mathbf{p}_n)\,J(\mathbf{k}_n)/\mathscr{J}]^{\frac{1}{2}}\sin\psi_n - G_i\{[J(\mathbf{k}_i)/J(\mathbf{p}_i)]^{\frac{1}{2}} - [J(\mathbf{p}_i)/J(\mathbf{k}_i)]^{\frac{1}{2}}\}\sqrt{\mathscr{J}}\sin\psi_i. \tag{4.1c}$$

The resonance condition (3.10) can be satisfied for $p_i < p_c$, the wavenumber at which the surface-wave group velocity is equal to the internal-wave phase velocity:

$$p_c = gK^2/(4\Omega^2). \tag{4.2}$$

Thus we include only those modes in (4.1) for which $p_c > p_i > k_0$.‡

Exact resonance is not required in (4.1) for significant transfer of excitation. To take account of this, we set $\omega_p - \omega_k - \Omega = -\delta f$, where δf represents the frequency mismatch. Now (3.11) becomes for a given wave vector $\mathbf{p}$

$$\mathbf{p}.\mathbf{K} \equiv pK\cos\beta = \tfrac{1}{2}[k^2 + K^2 - (f + \delta f)^4/g^2].$$

† Since α varies as $V_c^{-\frac{1}{2}}$ the curves in figure 3 are easily re-scaled for other values of V_c.

‡ For our numerical examples presented later, it can be verified that p_c lies below the range of capillary wavenumbers.

At exact resonance, corresponding to $\delta f = 0$, the angle β is β_r, where

$$\sin\beta_r \cong [1-p/p_c]^{\frac{1}{2}}. \tag{4.3}$$

For $\delta f \neq 0$, we have $\beta = \beta_r + \delta\beta$, and

$$\delta\beta \cong 2\omega_p \delta f/(gK\sin\beta_r). \tag{4.4}$$

The mode index i in (4.1) thus labels a magnitude and a direction for each $\mathbf{p}_i$.

Integration of (4.1) is simplified by introducing dimensionless variables, as follows: $J(\mathbf{p}_i) = Z_i J^0(\mathbf{p}_i), J(\mathbf{k}_i) = X_i J^0(\mathbf{k}_i), \mathscr{J} = \mathscr{J}_0 Y$, where [see (3.3)]

$$J^0(\mathbf{p}_i) = [(2\pi)^2 g\rho_0/A_0\omega_p]\Psi_s(\mathbf{p}_i) \cong J^0(\mathbf{k}_i), \tag{4.5a}$$

$$\mathscr{J}_0 = \frac{\rho_0 g'(j,K)}{\Omega}\Xi_0^2. \tag{4.5b}$$

Here Ξ_0 has the dimensions of length and is to be determined by the condition (4.7) below. A dimensionless time τ is introduced by the relation $t = \alpha^{-1}\tau$, where α is defined, as in § 3, by the equation

$$\alpha^2 = \sum_i [2G_i]^2 J^0(\mathbf{p}_i). \tag{4.6}$$

The constant Ξ_0 is then defined by the relation

$$2G_i \mathscr{J}_0^{\frac{1}{2}} = \alpha(p_i/p_c)^{\frac{3}{2}}. \tag{4.7}$$

This takes proper account of the dependence of G_i on p_i.

The scaling (4.5) for the action variables implies that for the assumed equilibrium surface-wave spectrum the initial values of the X_i and Z_i should be near unity.

To evaluate α^2, we start with the expression (3.12). If we make the arbitrary,† but reasonable, assumption that $|\delta f| \leqslant \alpha$, then (4.4) can be used to give

$$\int d\beta \mathscr{G}_s(p,\beta) = 4\omega_p\alpha/(\pi g K\sin\beta_r).$$

Integration over wavenumber, with the upper limit p_c (the lower limit k_0 can be taken to be zero for the present integration), gives

$$\alpha = [3{\cdot}2\times 10^{-2}\Omega^3(j,K)/\pi g'(j,K)\,K\sinh^2(KD)]. \tag{4.8}$$

The adopted scaling of variables in (4.1) leads to coefficients of order unity, removing the coupling strengths G_i and the dimensional quantities $J^0(\mathbf{p}_i)$ and $\mathscr{J}_0$. Writing $(2\pi)^2/A_0 = \delta p_x \delta p_y = p\,\delta p\,\delta\beta$ lets us carry out the mode number sums as a numerical integration.

Equations (4.1) were numerically integrated with the Z_i and X_i initially equal to unity (changing initial conditions showed this to be uncritical). Nine values for β and eight for p_i were used, making a total of seventy-two modes in (4.1). (Integration with fewer modes seemed to indicate little sensitivity to the number of modes used.)

A characteristic growth time τ_g for the internal-wave mode was defined as $\tau_g \equiv Y/\dot{Y}$, evaluated at that time τ that maximum power was being delivered

† Since α is a scale parameter, its precise definition is of course arbitrary.

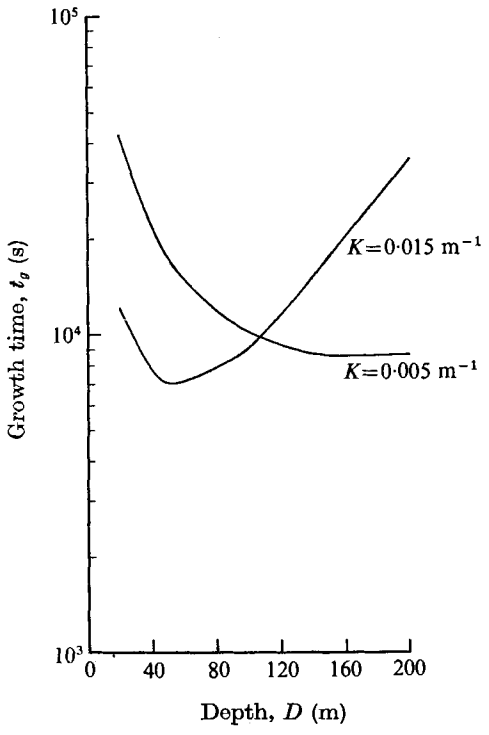

FIGURE 4. The growth time t_g [see (4.9)] is shown as a function of mixed-layer thickness for $\delta\rho/\rho_0 = 0$, mode 1 and internal wavenumbers of 0·015 m^{-1} and 0·005 m^{-1}.

to the internal wave (i.e. $\dot{Y}$ was a maximum).† It was found that $\tau_g = 0{\cdot}31$. This corresponds to a dimensional time

$$t_g = 0{\cdot}31\alpha^{-1}. \tag{4.9}$$

It might be noted that negligible transfer of excitation occurred for $\delta f > 10\alpha$. (The arbitrary choice $|\delta f| \leqq \alpha$ used in evaluating α is of course compensated in the numerical value for τ_g, since t_g is independent of this choice.)

Our dimensionless scaling of (4.1) was motivated by the simple model calculation of the last section. It is interesting to note that our elaborate numerical calculation is very close to the predictions of this earlier model based on the locked phase and parametric amplifier approximations.

To evaluate t_g using (4.8) and (4.9), the Garrett–Munk ocean model (1.2) and the internal-wave eigenmodes in the WKB approximation were again used. The resulting values of the growth time are shown in figures 4–7 for a range of parameters.

In figure 4 we show t_g (in seconds) as a function of the mixed-layer thickness D for the modes $j = 1$, $K = 0{\cdot}015$ m^{-1} and 0·005 m^{-1} and with $\delta\rho/\rho_0 = 0$.

In figure 5 we show t_g as a function of $\delta\rho/\rho_0$ for $D = 100$ m, $K = 0{\cdot}01$ m^{-1} and $j = 1, 2, 3$.

† For Y well below its saturation value the choice of time at which to evaluate τ_g was not very critical.

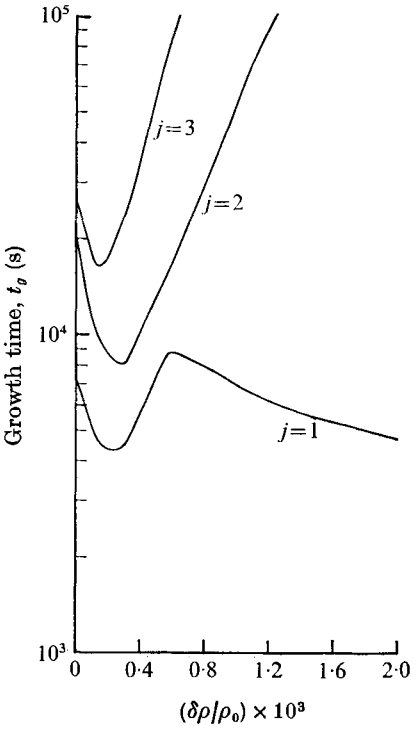

FIGURE 5. The growth time t_g [see (4.9)] is shown as a function of $\delta\rho/\rho_0$ for a mixed-layer thickness of 100 m, internal wavenumber 0·01 m^{-1} and modes $j = 1, 2, 3$.

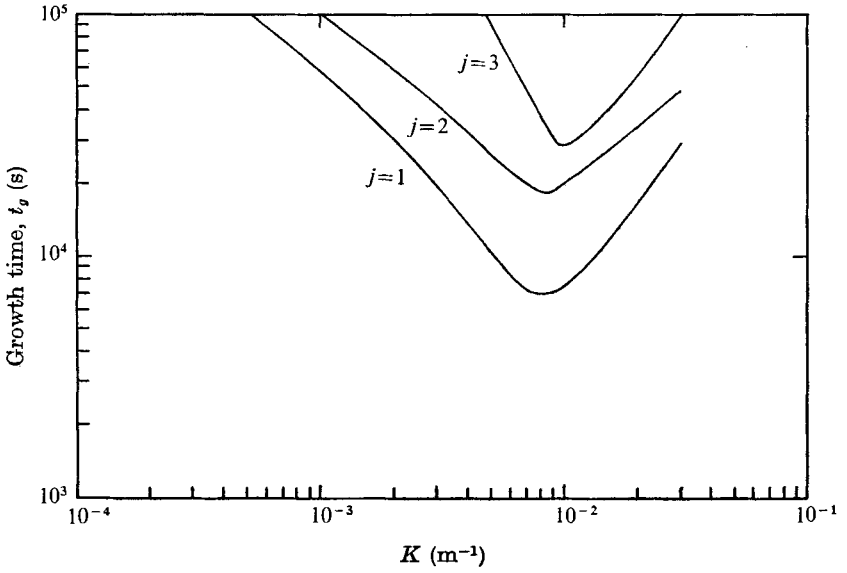

FIGURE 6. The growth time t_g [see (4.9)] is shown as a function of wavenumber for a mixed-layer thickness of 100 m, $\delta\rho/\rho_0 = 0$ and modes $j = 1, 2, 3$.

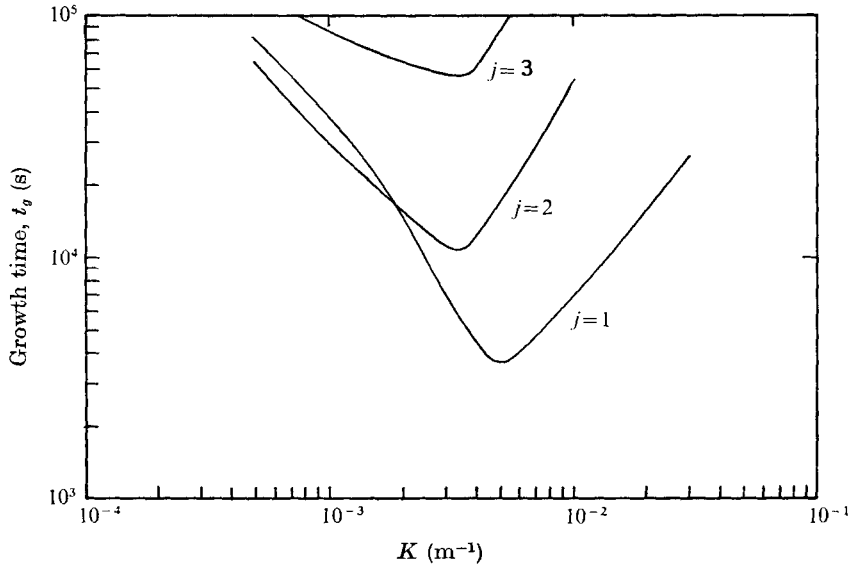

FIGURE 7. The growth time t_g [see (4.9)] is shown as a function of wavenumber for a mixed-layer thickness of 100 m, $\delta\rho/\rho_0 = 10^{-3}$ and modes $j = 1, 2, 3$.

Finally, in figures 6 and 7 we show t_g as a function of K for $j = 1, 2, 3$, $D = 100$ m, and $\delta\rho/\rho_0 = 0$ and 10^{-3}, respectively.

The weak excitation of the high-order modes is a consequence of their extending to greater depths than do the lowest modes. This greater depth increases the value of $g'(j, K)$ [see (2.30)] and thus reduces the coupling strength. [This is seen, for example, in (4.8).] The very weak coupling between surface and internal waves found by Kenyon (1968) is related to this observation. Kenyon used a constant Brunt–Väisälä frequency model, for which the internal wave extends to the ocean bottom, leading to a very large $g'(j, K)$ for all modes. Since the coupling interaction occurs near the ocean surface, the deeper the internal wave extends, the less effective the coupling appears to be. To test this conclusion, we evaluated $g'(j, K)$ for an $N =$ constant model (below $D = 100$ m) giving frequencies close to those of table 1. For $KD \lesssim 1$, we found g' to be between one and two orders of magnitude larger than that given by the Garrett–Munk model. The corresponding values of $\alpha(j, K)$ were at least an order of magnitude smaller than those given for mode $j = 1$ with the Garrett–Munk model. These conclusions are consistent with those of Joyce (1974), who noted that his two-layer model gave much stronger coupling than that found by Kenyon (1968).

The calculated interaction times given in figures 6 and 7 can be used to estimate the rate at which energy is fed to the internal-wave system by surface waves. Relation (3.3*b*) lets us write the power per unit area delivered to the internal waves of mode j as

$$P_j = \rho_0 \int g'(j, K)\, \Psi_I(j, \mathbf{K})\, d^2K/t_g. \tag{4.10}$$

We have evaluated this integral using the Garrett–Munk spectrum (3.6) with t_g taken from figure 6. The integration is restricted to the range $K > 7 \times 10^{-4}$ m^{-1},

since figure 2 (and our numerical calculations) suggests that when

$$K > 7 \times 10^{-4}\ \mathrm{m}^{-1}$$

the internal-wave energy per mode is too large to receive substantial energy from the surface waves. The results for $j = 1, 2$ are

$$P_1 \simeq 3\,\mathrm{erg/cm^2\,s}, \quad P_2 \simeq \tfrac{1}{2}\,\mathrm{erg/cm^2\,s}, \tag{4.11}$$

the principal contribution coming from the range

$$7 \times 10^{-4}\ \mathrm{m}^{-1} < K < 5 \times 10^{-3}\ \mathrm{m}^{-1}.$$

These transfer rates are surprisingly close to the value of about $1\,\mathrm{erg/cm^2\,s}$ obtained by Bell (1975) for considerations of internal tides. They are also not very dissimilar from the dissipation rate of approximately $7\,\mathrm{ergs/cm^2\,s}$ estimated by Garrett & Munk (1972*b*).

5. Discussion and conclusions

We have presented a theoretical model to calculate the energy interchange between surface and internal waves when both can vary. The surface-wave/internal-wave mode coupled equations are, of course, limited in their description of the energy transfer process in an oceanographic environment. The nonlinear interactions among surface waves, as well as among internal waves, have not been included in the model. Also, the coupling of the wind to the air–sea interface has been ignored. On the long time scale of the surface-wave/internal-wave interaction (characteristically several hours) these phenomena can significantly influence developing surface- and internal-wave spectra. However, in the equilibrium case, when the generation and dissipation (or transfer) rates of surface waves are not rapidly changing, the general conclusions based on the analysis and calculations describing the growth rates of the internal waves are thought to be useful. In particular the dependence of these rates on the wave vector $\mathbf{K}$, the depth of the pycnocline D, and the strength of density discontinuity at the pycnocline $\delta\rho/\rho_0$ for the lowest three modes $j = 1, 2, 3$ are thought to be of interest.

Equation (2.37) has also been tested against the experiments of Lewis *et al.* (1974) and Joyce (1974) in Watson *et al.* (1975) and the agreement is quite good. In the experiments of Lewis *et al.* the modulation in amplitude and slope of a mechanically generated surface wave interacting with a constant amplitude internal wave was recorded. Matching the group velocity of the surface wave with the phase velocity of the internal wave forms a resonance in the system, thereby inducing a strong energy transfer. Numerically integrating (2.37) reproduces the results of linear theory at early times, but shows a tendency for the modulation to approach a maximum value at late times owing to the nonlinear frequency shift in the surface wave. The experimental points, however, do not extend into this nonlinear regime.

Joyce (1974) experimentally excited an internal wave along a density discontinuity by the resonant interaction of two driven surface waves and records

Surface waves	($0{\cdot}0298\ \mathrm{m}^{-1}$, Θ_n),	($0{\cdot}030\ \mathrm{m}^{-1}$, Θ_n)
	($0{\cdot}0302\ \mathrm{m}^{-1}$, Θ_n),	($0{\cdot}0304\ \mathrm{m}^{-1}$, Θ_n)
Internal waves	($4\times10^{-4}\ \mathrm{m}^{-1}$, 90°)	($4{\cdot}47\times10^{-4}\ \mathrm{m}^{-1}$, 63·4°)
	($6\times10^{-4}\ \mathrm{m}^{-1}$, 90°),	($6{\cdot}32\times10^{-4}\ \mathrm{m}^{-1}$, 71·6°)
	($8\times10^{-4}\ \mathrm{m}^{-1}$, 90°),	($8{\cdot}2\times10^{-4}\ \mathrm{m}^{-1}$, 78°)
	($10^{-3}\ \mathrm{m}^{-1}$, 90°),	($1{\cdot}02\times10^{-3}\ \mathrm{m}^{-1}$, 78·7°)
	($1{\cdot}2\times10^{-3}\ \mathrm{m}^{-1}$, 90°),	($1{\cdot}217\times10^{-3}\ \mathrm{m}^{-1}$, 80·5°)

TABLE 2. The wave vectors for twenty-four surface modes are listed, where for each wavenumber k there are six angles given by $\Theta_n = -3{\cdot}8°n$, $n = 0, 1, \ldots, 5$. Also listed are ten internal modes in polar co-ordinates.

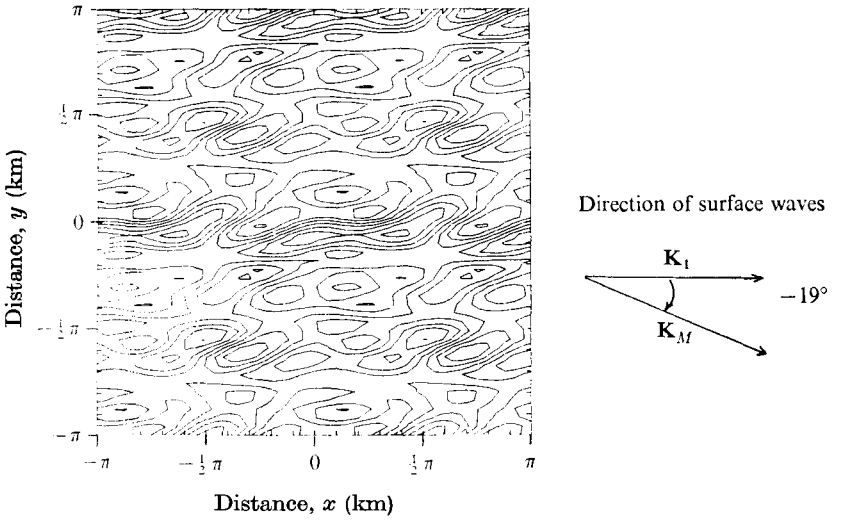

FIGURE 8. Contours of equal surface-wave height are shown in the two-dimensional horizontal plane of the ocean surface at time $t = 0$ for the twenty-four surface modes in table 2. The direction of propagation of the surface waves is indicated by the cone.

the growth in internal-wave amplitude. The theoretical calculation of the growth of the internal wave uses an extension of a theory due to Thorpe (1966). In our formulation this theory is equivalent to 'locking' the phase $\psi(\mathbf{k}, 1, \mathbf{K})$ to the value π. A modest improvement over Joyce's calculation was obtained by an integration of the complete set (2.37) in Watson *et al.* (1975).

A constant Brunt–Väisälä frequency was used by Kenyon (1968) to study the coupling between surface and internal waves. We concluded in §4 that this model leads to a very much weaker coupling than either the Garrett–Munk or the two-layer model (already observed by Joyce 1974) and is presumably unrealistic for studying the generation of internal waves by surface waves.

In § 2 the possible existence of a 'cascade' process of energy exchange resulting from a matching of the internal-wave phase velocity and the group velocity of the surface-wave spectrum was discussed using a simple model. Such a process has been observed in another context by Cohen *et al.* (1972). The total energy

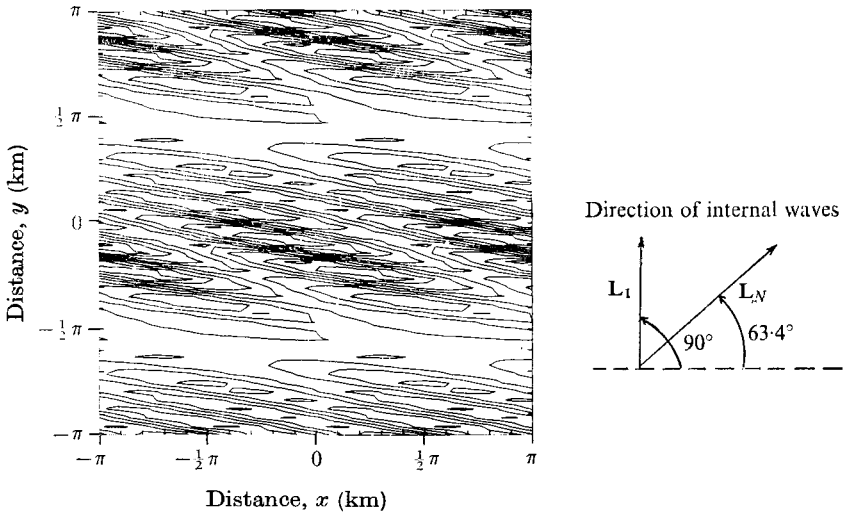

FIGURE 9. Contours of equal internal-wave height are shown in the two-dimensional horizontal plane of the ocean surface at time $t = 0$ for the ten internal modes in table 2. The direction of propagation of the internal waves is indicated by the cone.

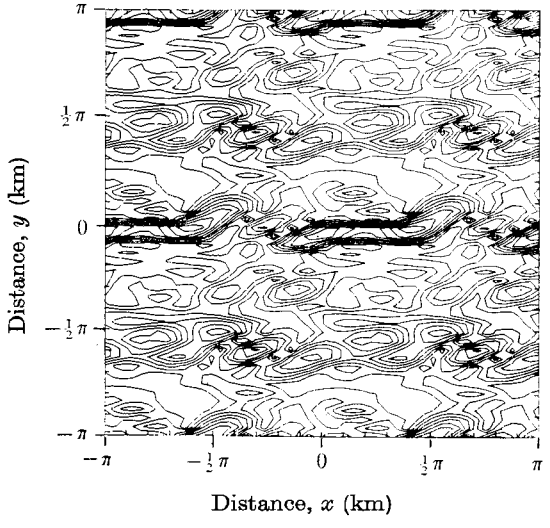

FIGURE 10. Contours of surface-wave slope are shown in the two-dimensional horizontal plane of the ocean surface at time $t = 200$ s for the twenty-four surface modes in table 2.

transfer rate from the surface- to the internal-wave spectrum based on the more general results of §4 is found to be comparable to estimates made by Bell (1975) and Garrett & Munk (1972*b*) for other processes.

Until now our attention has been focused on the energy transfer from surface to internal waves via the resonant triad interaction with the exception of the brief comments relating to the experiments of Lewis *et al.* A few remarks on the modulation of a surface-wave 'spectrum' by a spectrum of internal waves is probably of interest.

We model the ocean environment with 24 surface modes and 10 internal modes with the wave vectors shown in table 2. In this case, in addition to the surface waves having the equilibrium amplitudes prescribed by (3.4), the internal-wave amplitudes are given by the Garrett & Munk spectrum (3.6). In figures 8 and 9 a two-dimensional view of contours of equal surface- and internal-wave height, respectively, are depicted. In figure 8, we see that the surface waves are travelling in a 19° cone from left to right and produce a weak interference pattern in approximately the transverse direction.

In figure 9 the internal waves are seen to propagate at approximately right-angles to the surface waves, also with a definite pattern.

The intensity of incoherent light back-scattered from the ocean surface is dependent on the mean-square surface slope. In figure 10 contours of equal surface slope, i.e. $|\nabla\zeta_g|$, are shown. By averaging the slope contours in this figure over a length large compared with the surface-wave wavelengths and small compared with the internal-wave wavelengths, one obtains a measure of the 'visibility' of the internal-wave pattern. The contours are plotted at 200 s to give the surface-wave field time to respond to the internal waves.

The small-scale structure in figure 10 is qualitatively similar to the 'mottling' of the ocean surface observed in satellite photographs, by Apel *et al.* (1975*a*), taken from the ERTS1 satellite. This effect arises from the self-interference of the surface waves and is enhanced by the interaction with the internal waves.

The authors would like to thank Dr Walter Munk for several discussions and comments concerning this work. They would also like to thank Dr John Apel for both correspondence and discussions concerning the ERTS satellite observations. Finally, the authors thank the referees for suggestions which have hopefully made the paper more readable. This research was partially supported by the Defense Advanced Research Projects Agency (DARPA), 1400 Wilson Boulevard, Arlington, Virginia 22209, and monitored by the Air Force Systems Command, Rome Air Development Center, Griffiss Air Force Base, New York 13440, under Contract F30602-72-0494.

REFERENCES

Apel, J. R., Byrne, H. M., Proni, J. R. & Charnell, R. L. 1975*a* *J. Geophys. Res.* **80**, 865.

Apel, J. R., Proni, J. R., Byrne, H. M. & Sellers, R. L. 1975*b* *Geophys. Res. Lett.* (to appear).

Ball, F. K. 1964 *J. Fluid Mech.* **19**, 465.

Bell, T. H. 1975 *J. Geophys. Res.* **80**, 320.

Cohen, B. I., Kaufman, A. N. & Watson, K. M. 1972 *Phys. Rev. Lett.* **29**, 581.

Garrett, C. & Munk, W. 1972*a* *Geophys. Fluid Dyn.* **3**, 225.

Garrett, C. & Munk, W. 1972*b* *Deep-Sea Res.* **19**, 823.

Garrett, C. & Munk, W. 1975 *J. Geophys. Res.* **80**, 291.

Hasselmann, K. 1966 *Rev. Geophys.* **4**, 1.

Joyce, T. M. 1974 *J. Fluid Mech.* **63**, 801.

Kenyon, K. 1968 *J. Mar. Res.* **26**, 208.

LEWIS, J. E., LAKE, B. M. & KO, D. R. S. 1974 *J. Fluid Mech.* **63**, 773.

NISHIKAWA, K. 1968 *J. Phys. Soc. Japan*, **24**, 916.

PHILLIPS, O. M. 1966 *The Dynamics of the Upper Ocean.* Cambridge University Press.

THORPE, S. A. 1966 *J. Fluid Mech.* **24**, 737.

THORPE, S. A. 1975 *J. Geophys. Res.* **80**, 328.

TYLER, G. L., TEAGUE, C. C., STEWARD, R. H., PETERSON, A. M., MUNK, W. & JOY, J. W. 1974 *Deep-Sea Res.* **21**, 989.

WATSON, K. M., WEST, B. J. & COHEN, B. I. 1975 Coupling of surface and internal gravity waves: a Hamiltonian model. *Phys. Dyn. Rep.* PD-73-032, RADC-TR-74-129.

WHITHAM, G. B. 1974 *Linear and Nonlinear Waves.* Wiley.